# An ion beam reflectron/single-photon infrared emission spectrometer for the study of gas-phase polycyclic aromatic hydrocarbon ions: Testing proposed carriers of the unidentified infrared emission bands

Hack-Sung Kim[a] and Richard J. Saykally[b]
*Department of Chemistry, University of California, Berkeley, California 94720-1460*

(Received 18 July 2002; accepted 11 December 2002)

We describe the design and performance of an electron-impact ion beam reflectron system coupled to our ''single-photon infrared emission spectrometer'' for measurement of infrared emission from excited gas-phase polycyclic aromatic hydrocarbon (PAH) cations. This experiment provides for direct comparison of laboratory infrared emission spectra of gaseous ionized PAHs with the ''unidentified infrared emission bands,'' the origin of which is still debated. © *2003 American Institute of Physics.* [DOI: 10.1063/1.1544418]

## I. INTRODUCTION

Our group has developed an infrared photon-counting experiment based on a blocked impurity band-solid state photomultiplier (BIB-SSPM)[1] to measure gas-phase IR emission from UV laser excited neutral polycyclic aromatic hydrocarbons (PAHs) over the entire spectral region spanned by the ''unidentified infrared emission bands (UIRs).'' [2] We call this technique single-photon infrared emission spectroscopy (SPIRES),[3,4] since a single incident IR photon is capable of generating a measurable voltage pulse. With this experiment, we have examined IR *emission* spectra of a large collection of neutral PAHs, finding that none of them are likely to be a major contributor to the UIRs.[3–5] To effectively use the BIB-SSPM, the detector must be cooled below ~7 K and shielded from blackbody radiation emitted by the surroundings. Since the detector is saturated at count rates near $10^8$ photons/$(s\,cm^2)$, the entire spectrometer must be maintained at temperatures lower than ~15 K.[6]

IR spectral features of PAH cations have been studied by IR, matrix isolation IR absorption spectroscopy, and theory and PAH cations are currently thought to be more probable candidates for carriers of the UIRs than neutral PAHs.[7–9] However, due to the strong matrix perturbations expected for ionic molecules, as well as the dependence of IR frequencies on the vibrational temperatures of the ground electronic state of excited PAHs, gas-phase emission measurements are necessary to definitively test PAH proposals.[2,10] Recently, Oomens *et al.*[11,12] have developed an *absorption* experiment based on photodestruction of trapped *gas-phase* ions, wherein the internal energy-dependent redshifts in vibrational transitions are measured by controlling the trapping time. Our gas-phase emission measurements, as well as these gas-phase absorption measurements, are thus capable of contributing definitive new insights into the origin of the UIRs.

The direct detection of *mid-IR emission* from *gas-phase ions* is a formidable technical challenge. Typical ion currents (~2 $\mu$A at the field of view of the monochromator in the SPIRE spectrometer) correspond to number densities of only $10^6$–$10^7$ $cm^{-3}$ (or correspond to ~$10^{-12}$ Torr using the ideal gas law). Also, the average lifetime of gas-phase ions (without an ion trap) is usually short (~$10^{-5}$ s in our system). Moreover, all optical elements in the field of view of the detector must generate a negligible blackbody photon flux over the entire spectral region of interest in order to effectively use the BIB-SSPM. Hence, ion optics in the field of view of the detector must be cooled to ~77 K and the diameter of the ion beam aperture in the field of view of the detector must be minimized. Since the space charge limited ion current is inversely proportional to the square root of molecular mass, the maximum achievable ion current of molecules with high molecular mass (e.g., PAHs) is lower than that of molecules with low mass, for constant aperture. Therefore, it is difficult to achieve a current density of excited PAH ions at the final aperture in the field of view of the detector that is high enough to yield detectable mid-IR emission in the cryogenic environment.

Nevertheless, we recently reported the observation of gas-phase IR emission spectra from excited PAH cations.[13] The measured SPIRE spectrum of the pyrene cation ($C_{16}H_{10}^+$) agrees well with the general appearance of the UIR features, thus providing support for the role of the cations in the ''PAH hypothesis.'' [2,10] Here we describe the detailed design and performance of the electron-impact ion beam reflectron system coupled to the SPIRE spectrometer that was used to detect the infrared emission of gas-phase ions in the mid-IR region.

## II. EXPERIMENTAL DESIGN

### A. Ion beam system and SPIRE spectrometer interface

A number of stringent requirements were placed on the design of the PAH ion beam system: maximum current density of ions, minimum blackbody emission from the (room temperature to liquid $N_2$ temperature) surroundings, sepa-

[a]Present address: Institute for Environmental Catalysis, Northwestern University, Evanston, IL 60208; electronic mail: hskim@northwestern.edu
[b]Author to whom correspondence should be addressed; electronic mail: saykally@uclink.berkeley.edu

 

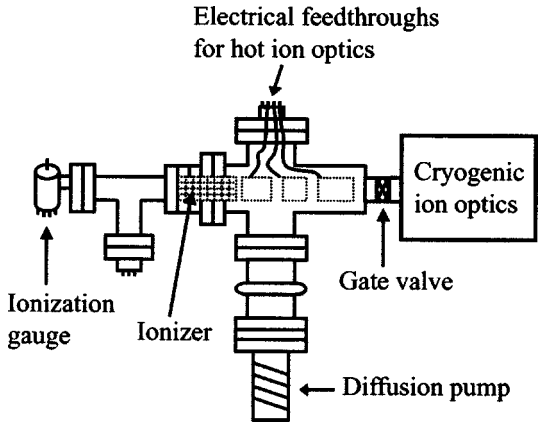


FIG. 1. Ion beam vacuum chamber (ionizer and hot ion optics region).

rated vacuum systems, and cryogenic electrodes and insulators with high thermal conductivity.

The ion beam system was designed to interface directly with the cryogenic sample Dewar of the existing SPIRE spectrometer, while retaining the complete functionality of the laser desorption setup.[3–6] The sample Dewar is attached to a lead screw and rail bearings so that it can be interfaced via interlocking baffles with the monochromator. A support for the ion beam was constructed with rails that would allow the entire ion beam apparatus to translate along with the sample Dewar.

The ion beam vacuum system diagrammed in Fig. 1 was constructed from 2.5 in. o.d. stainless steel tubing. A cross at one end holds the ion gun along one axis and a 2 in. diffusion pump below. The end of the chamber has a welded ISO NW 25 quick flange that connects to a miniature gate valve (see the gate valve in Figs. 1 and 3), which separates the ''hot'' ion optics from the cryogenic sample Dewar. The gate valve and separate vacuum systems allow for access to the ion gun without requiring warming and venting of the sample Dewar, while the ISO quick-connect flanges at the gate valve facilitate rapid disassembly during the testing and development of the ion beam.

### B. Generation of PAH ions and hot ion optics design

PAH ions were generated by electron-impact ionization of thermally generated PAH vapor. It is well known that a single molecular ion peak dominates the mass spectrum of ionized PAH generated by electron-impact ionization, as a consequence of the high activation energies required for fragmentation. The primary ionic species produced for peri-condensed PAHs like pyrene[14] is thus the parent monocation ($C_{16}H_{10}^{+}$), followed by the dehydrogenated cations ($C_{16}H_{9}^{+}$, $C_{16}H_{8}^{+}$, etc.), and the dications ($C_{16}H_{10}^{2+}$, $C_{16}H_{8}^{2+}$).

The expected physical state of interstellar PAHs emitting the UIRs excited by the absorption of UV (or far UV)[15] photons corresponds to vibrationally hot[16] (~900 K) and rotationally cold[17] (~100 K) molecules. Unanswered questions at the outset of the PAH ion beam experiments were whether the molecules would become sufficiently vibrationally excited by the electron-impact event and whether the electron-impact excitation would resemble the absorption of UV photons. We show that this is indeed the case.

Classically, electron impact behaves like a short pulse light source, in view of a time-dependent electric field interacting with the molecule.[18] The typical effective pulse duration is subfemtosecond, and it is well established that electron-impact excitation mimics photoabsorption (optical dipole excitation) at high impact energies.[19] High vibrational excitation was observed in benzene[20] and coronene[21] and it is a general characteristic of electron-impact ionization. Maier and Marthaler[22] observed IR emission spectra from electron-impact ionized *p*-dichlorobenzene cation. The electronically excited PAH (ion) relaxes by rapid internal conversion to the ground electronic state, and the electronic energy is then distributed among the various vibrational modes (internal vibrational redistribution, IVR). The vibrational temperature of the *ground* electronic state of the PAH ion (on which IR emission will occur) after IVR, produced by electron impact in effusive beam, can also be determined empirically. IVR has been observed in the electron-impact excited emission spectrum of *p*-difluorobenzene[23] as well as in laser experiments.[24] Therefore, we can conclude that electron-impact excitation mimics photoabsorption reasonably closely in the present context, and also should approximate the UIR mechanism,[10] except for the low rotational temperature.[17] In our experiments, the rotational temperature is estimated to be near the oven temperature (~340 K). We will discuss it later.

A small oven for vaporizing PAH molecules was made from 1/2 in. o.d. stainless steel tubing, mounted outside of the ion beam vacuum shield, and heated with resistive heating tape. The stainless steel tubing was kept as short as possible between the oven and the ionizer. An oxygen-free high conductivity (OFHC) copper sleeve was inserted and welded inside the stainless tubing to minimize the condensation of the sample inside the wall, which also facilitates thermal conduction during sample heating. The optimal temperature for vaporization of pyrene was found to be 70–75 °C, at which the pyrene vapor pressure is estimated[25] to be approximately $(1.0–1.5)\times10^{-2}$ Torr. The pressure measured in the ionization region of the ion beam was $(5–10)\times10^{-5}$ Torr during experiments.

The ionizer and extraction electrodes used in this work are similar to the ion gun designs described elsewhere.[26] A commercial nude ionization gauge (Varian, UHV-24) with a dual tungsten filament and a thin grid was used as an ionizer ($Ir/ThO_2$ filament is vulnerable to PAHs). A very thin grid decreases the probability of collision between the positively biased grid and electrons. Since the bottom end of the grid cage, in which ions are created, is closed, the relatively constant electric field reduces their kinetic energy spread.

The ion gauge was modified in the following ways: The central ion collector was removed, and a hole was drilled in the back of the gauge to allow for the insertion of the PAH oven. The top end of the wire cage was removed to make space for the extraction electrodes, and the gauge was surrounded by a stainless mesh (''the repeller'') and was electrically connected to the filament. The repeller increases the lifetime (or pathlength) of electrons, and thus the probability

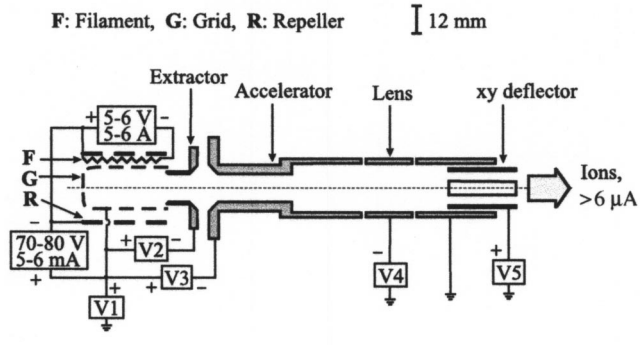


FIG. 2. The SPIRES ion gun and hot ion optics: Vaporized pyrene molecules are ionized by 70–80 eV electrons, yielding an ion beam with ion currents of at least 6 $\mu$A and 1 keV beam energy at the entrance aperture of the cryogenic ion optics system.

of electron collision with neutral pyrene molecules.

The filament is heated with a 5–6 A current and the electron emission current was 5–6 mA, as shown in Fig. 2. The grid is held at +1000 V with respect to the ground. The repeller and filament are held at −70 to −80 V with respect to the grid, giving rise to 70–80 eV electron energies. All electrical connections for the ion gun were made through standard metal-ceramic feedthroughs on flanges behind the ionizer.

The ions generated in the ionizer are attracted toward the extraction and acceleration electrode, which are held at ~−195 and −555 V with respect to the grid, respectively. The tubular extraction, and acceleration and lens electrodes, are mounted on a stainless steel cage attached to a 4.5 in. flange, and alumina spacers provided electrical insulation. The extractor field contours are concave, directing the ions towards the beam axis, while the conical shape of the first two electrodes simulates a tube lens with a large effective radius. The first focusing of the ion beam is accomplished with the lens held at approximately −2100 V with respect to the ground, operated as an asymmetrical Einzel lens. The electrical connections are diagrammed in Fig. 2.

Ion currents of at least 6 $\mu$A at the entrance aperture of the cryogenic ion optics were measured behind a 6-mm-diam aperture at a distance of 56 mm from the end of the "*xy* deflector" at 1 keV beam energy. The *xy* deflector at the exit of the ion gun was used to deflect the ion beam during background IR emission measurements. One of four electrodes is held at +500 V with respect to the ground, and the others are electrically tied to the ground. The ion current at the entrance aperture of the cryogenic ion optics was essentially zero (less than 2 nA) when the deflecting voltage was applied. The potentials used for the ion beam electrodes are listed in Table I.

TABLE I. Typical electrical potentials for PAH ion beam. All the potentials except for $V_{grid}$ are determined by SIMION ion beam simulations (see Ref. 28 and Fig. 6) and by the optimized ion current measurements using sequential Faraday cups located: at the entrance aperture of transfer lens, at the entrance aperture of the quadrupole deflector (QD), at the straight aperture of the QD, at the exit aperture of the QD, and at the last ring of the reflectron.

| Reference | Notation | Electrode | Voltage applied[a] |
|---|---|---|---|
| Figure 2 | $V1=V_{grid}$ | Ionizer grid | +1000 |
| | $V2=V_{extr}$ | Extraction | +805 |
| | $V3=V_{acc}$ | Acceleration | +445 |
| | $V4=V_{lens}$ | Lens | −2100 |
| | $V5=V_{xy}$ | *xy* deflector (one of four electrodes) | 0 or +500 |
| Figure 3 | $V6=V_{trans}$ | Transfer lens | +914 |
| Figure 4 | $V_{QD-}$ | Quadrupole deflector | −770 |
| | $V_{QD+}$ | | +1300 |
| Figure 5 | $V_{R1}$ | Reflectron region | +950 |
| | $V_{R2}$ | | +300 |
| | $V_{R3}$ | | +50 to +700 |
| | $V_{R4}$ | | +100 to +2300 |
| | $V_{R5}$ | | 0 or +2100 |

[a]All the voltages are with respect to the ground.

### C. Cryogenic ion optics

Electrostatic ion beam optical systems are normally constructed of stainless steel electrodes, electrically isolated from one another with ceramic standoffs and spacers. However, neither of these materials has sufficient thermal conductivities to allow for rapid and efficient cooling to the temperatures required for SPIRE measurements. Oxygen-free high conductivity (OFHC) copper is the material of choice for high thermal conductivity and all the cryogenic electrodes in the ion beam system are made from OFHC copper. Electrically isolating the ion optics while still allowing them to cool efficiently was a formidable design challenge. All the cryogenic electrical insulators (with high thermal conductivity) between the cryogenic OFHC copper electrodes are made from boron nitride. Stainless steel and G-10 (a machinable epoxy-paper laminate) were used for mechanical connections when low thermal transport was required.

#### 1. Transfer lens

The transfer lens is the first cryogenically cooled lens in the beam path attached to the inner shield of the sample Dewar. This lens also served as an IR spatial filter. It was placed between the gate valve (separating the ion extraction chamber from the cold sample Dewar) and the quadrupole deflector in the center of the sample Dewar. This was a very tight space in which to fit a three-electrode symmetrical Einzel lens. The maximum usable diameter of three electrodes is approximately 0.9 in. in order to maintain multi-use functionality of the sample Dewar. The length of the central tube electrode is designed to be the same as the inner diameter of the tube to minimize both cushion and barrel distortion.[27] The device we ultimately employed is diagrammed in Fig. 3. The design of the transfer lens was assisted by the SIMION ion beam simulation program.[28]

The transfer lens is made in four pieces: stainless steel entrance aperture, OFHC copper entrance and exit apertures, and (OFHC copper) central electrode. The stainless steel entrance aperture was welded into a homemade flange located between the gate valve and the transfer lens in order to minimize the radiative heat load on the sample Dewar. The lens in the ionizer chamber was designed to focus at this aperture. The OFHC copper entrance aperture screwed into a female-threaded copper flange on the liquid nitrogen (Liq. $N_2$)

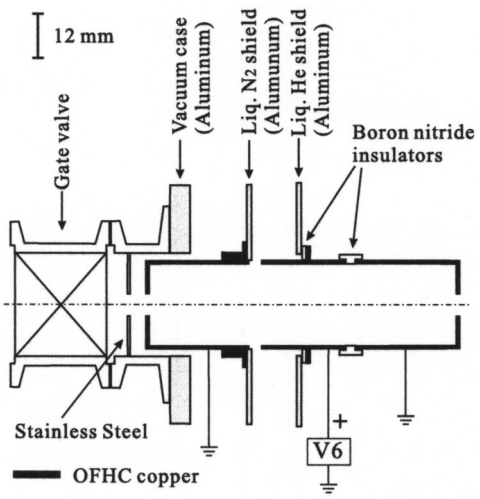


FIG. 3. Einzel transfer lens cooled to 77 K during experiments.

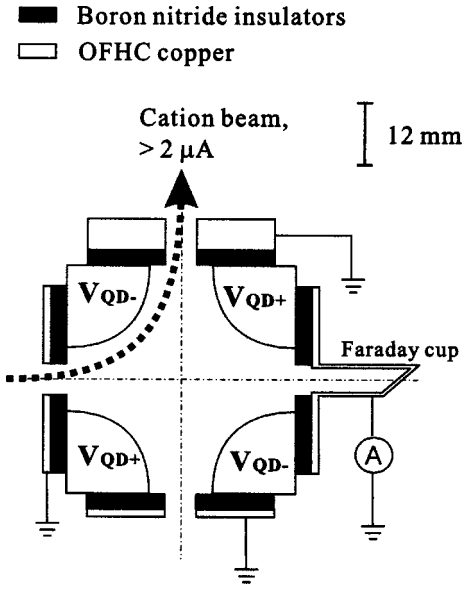


FIG. 4. Quadrupole deflector cooled to 77 K during experiments: Boron nitride insulator disks (1.5 in. diameter) and OFHC copper electrodes were used to simultaneously maximize electrical insulation and thermal conductivity.

shield to minimize the radiative heat load on the inner shield. This allowed for easy removal during the iterative design and testing process. An additional G-10 spacer surrounds the outside of the OFHC copper entrance aperture to keep the part centered on the beam axis, as the thin cold shields tend to drift upon cooling. The central electrode was connected on the Liq. He shield using ceramic screws. A boron nitride spacer is inserted between them. The central electrode is isolated from the exit aperture and from the Liq. He shield with boron nitride spacers. The entrance and exist apertures, the Liq. $N_2$ shield, and the Liq. He shield are electrically tied to the ground. The potentials used for transfer lens electrode are listed in Table I.

### 2. Quadrupole deflector

The most important and challenging design consideration of the SPIRES ion beam was to efficiently direct the ion beam along the viewing axis of the monochromator (toward the entrance slit), without exposing any hot surfaces (room temperature to high temperature vacuum walls due to the hot filaments of the ionizer, etc.) to the spectrometer field of view. This was accomplished with an electrostatic quadrupole deflector, which can turn an ion beam 90° without incurring appreciable energy or angular spread.[29] Ding and Richter[30] used a 90° deflection magnet to measure laser-induced fluorescence of an $N_2$-ion beam produced in a plasma ion source. Unlike magnetic sector deflectors, it is neither mass selective nor requires high-current power supplies. The electrostatic quadrupole deflector was an obvious choice, since it had been characterized and used in previous experiments (Direct Laser Absorption Spectroscopy in a Fast Ion Beam) by Owrutsky *et al.*[31] For cryogenic operation, the parts of the quadrupole deflector were constructed entirely from OFHC copper, electrically isolated with boron nitride disks, and held together with nylon or ceramic screws.

The entrance and exist apertures on the device must be kept small to avoid large fringing fields, which act as lenses and distort the beam. Auxiliary shim electrodes were generally used in order to prevent the fringing fields from causing significant aberrations,[29] but a simpler quadrupole deflector without the shim electrodes whose aberrations are negligible has been reported.[32] If grounded apertures are installed just before the entrance to the quadrupole and just after the exit, it confines the fringing fields to a short region. In our experiment, when grounded apertures were installed, it was found that higher ion currents could be achieved at the exit aperture of the quadrupole deflector without using the shim electrodes shown in Fig. 4. The potentials used for the quadrupole deflector are listed in Table I.

### 3. Reflectron

When existing the quadrupole deflector, the ion beam enters the field of view of the cryogenic monochromator, traveling toward the entrance slit. Here, a series of ring electrodes made from OFHC copper are arranged between boron nitride ring spacers comprising the remaining beam shaping and reflectron optics (Fig. 5). The design of the reflectron was facilitated by use of the SIMION ion beam simulation program.[28] The electrodes were stacked in this way (as opposed to having vacuum gaps between electrodes) to ensure adequate cooling of this long extension, which was mounted directly on the quadrupole deflector. A silicon diode (DT 470), as is shown in Fig. 5, measures the temperature.

The (A) ring electrode in Fig. 5 is divided into two parts. One electrode is electrically tied to the ground and the other is positive with respect to the ground by up to $V_{R3}$. The (B) electrode, the last ring of the stack (closest to the monochromator), is also divided into two parts. The design of this part of the beam is quite flexible. It was originally conceived as a simple reflection field, which would reflect the ions away from the monochromator, increasing ion residence time in the viewing region (when $V_{R4} \approx 2300$ V). However, instead of just reflecting the beam, the beam can be deflected into a Faraday cup for final beam characterization and *in situ* beam monitoring (when $V_{R4} < 1000$ V and $V_{R5} \approx 2100$ V). The potentials used for the ring electrodes are listed in Table I.

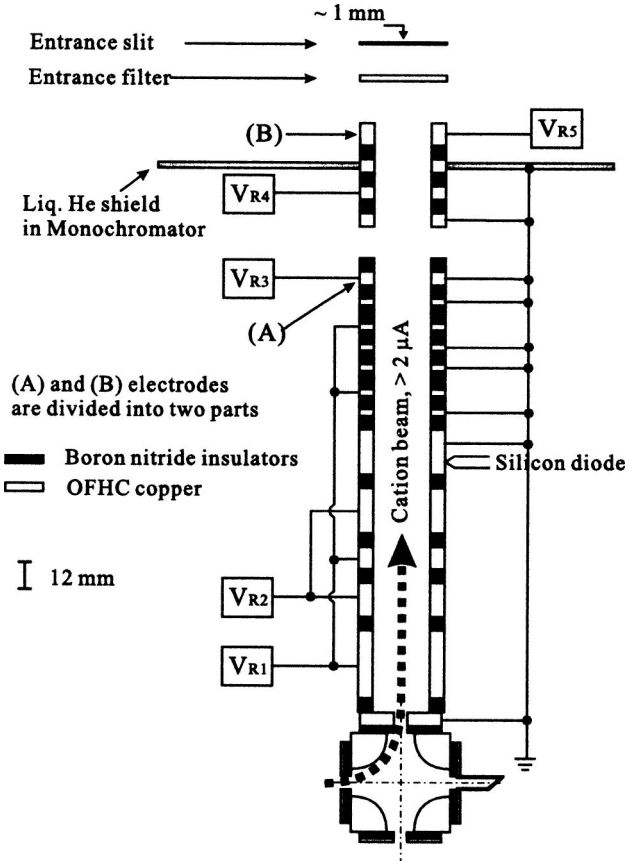


FIG. 5. Reflectron cooled below 77 K during experiments: The last ring of stack [R4, R5, (B) electrodes and their electrical isolators, boron nitrides] are contacting with Liq. He shield cooled to liquid He. A series of boron nitride insulator disks (1.5 in. diameter) are arranged between OFHC copper ring electrodes (1.5 in. diameter) to simultaneously maximize electrical insulation and thermal conductivity.

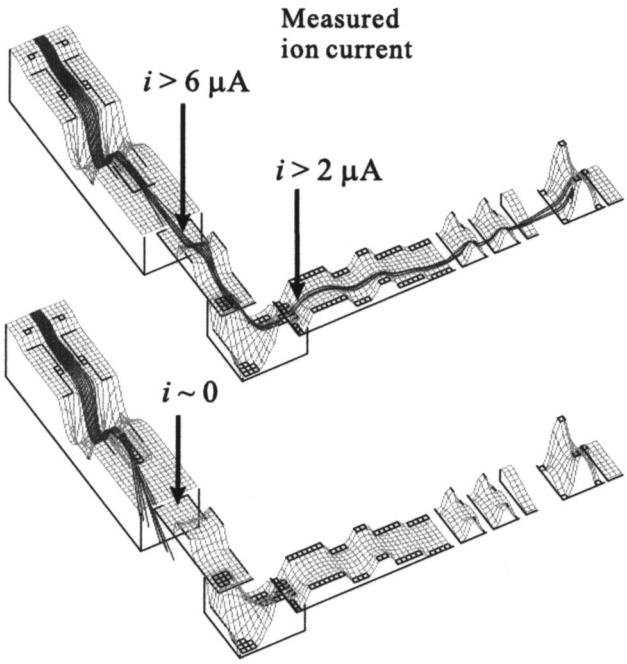


FIG. 6. SIMION ion beam simulations (Top: Ion beam trajectory during signal measurement. Bottom: Beam trajectory during background measurement.). The trajectories are based on the observation of the ion current using a homemade Faraday cup. The *xy* deflector is switched to +500 V, steering the beam away from the sample Dewar aperture. The measured ion currents shown were collected at 1 keV energy.

### D. Signal generation and collection

We used the same equipment as for the PAH desorption experiments.[3–6] The SRS 430 multichannel scaler was set up to collect signal for some amount of time (typically 10 s) while ions were present in the monochromator field of view [see Fig. 6 (top)]. The photon counts were summed by the instrument as a function of wavelength ($\Delta x$ is typically 0.005 $\mu$m) and sent to the computer. During the background scan, the ion beam was deflected with a +500 V potential at the *xy* deflector [see Fig. 6 (bottom)] and the ion current in the reflectron was less than 2 nA. The photon counts during the background scan were also summed, transferred, and subtracted from the signal scan.

The data collection program was written[6] in LabView version 4.0 (http://www.ni.com, National Instruments) and the data collection times had to be quite long as a result of the low ion concentration and the low spontaneous emission rate of PAH ions at IR wavelengths. The IR radiative emission rate for PAH ions is conservatively estimated[33] at 100 $s^{-1}$, while the ion current in the reflectron region of the beam exceeds 2 $\mu$A at 1 keV. With this information, it is possible to estimate the signal collection times required to achieve a reasonable signal to noise ratio. While a 2 $\mu$A beam current implies a flow rate of $1.2\times10^{13}$ ions/s into the reflectron viewing region, we estimate that 50% of those ions are the cation of interest ($6\times10^{12}$ ions/s). Assuming that as few as 50% of those are vibrationally excited, the rate of production of excited cationic pyrene, which will emit IR radiation, will be as low as $3\times10^{12}$ ions/s. The residence time of a 1 keV ion in the reflectron is estimated at $\sim10^{-5}$ s. Therefore, the photon emission rate will be $\sim3\times10^{9}$ photons/s in the reflectron region for a spontaneous emission coefficient of 100 $s^{-1}$. The collection efficiency of light from the ion beam is not rigorously determined, but is limited by the spectrometer étendue (slit area$\times$solid angle), and is estimated to be $\sim10^{-6}$. Coupled with the efficiency of the BIB-SSPM detector (estimated at 5%), we would record about 150 photons/s ($=R_S$).

The dark count rate ($=R_D$) of the BIB-SSPM detector is typically less than 2000 counts/s. The signal to noise ratio of the detection system can be expressed as $\mathrm{S/N}=R_S\sqrt{t}/\sqrt{(R_D+R_S)}$, where $t$ is the signal integration time. It is thus estimated that a signal collection time of 10 s is required to achieve S/N$\cong$10, and that level of performance is actually realized in these experiments on PAH ions. These results were described in a recent article,[13] and we will discuss a brief analysis of the SPIRE spectra in the following section.

## IV. RESULTS

The SPIRE spectrum in Fig. 7(b) was obtained in the 5.5–8.5 $\mu$m region when the ions generated by the electron impact of pyrene vapor were injected into the reflectron region (see Figs. 5 and 6). The SPIRE background spectrum in

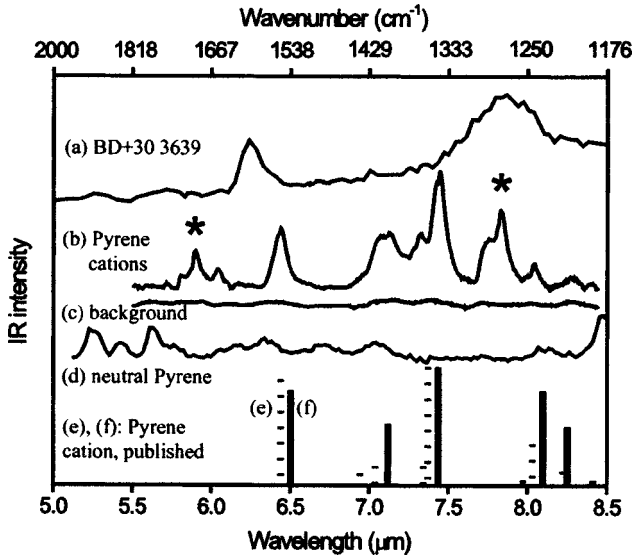


FIG. 7. SPIRE spectrum of gas-phase pyrene cations ($C_{16}H_{10}^{+}$ and etc.) in the 5.5–8.5 $\mu$m region when the pyrene vapor pressure was relatively low ($1.0\times10^{-2}$ Torr): Trace (b) is the observed SPIRE spectrum of gas-phase pyrene cations with the background subtracted, corrected for monochromator (filters, mirrors, a diffraction grating and a detector) throughput and its intensities are normalized. Trace (c) is the background spectrum. Trace (d) is the gas-phase SPIRE spectrum of neutral pyrene reported previously (see Ref. 4). The IR absorption spectra for the pyrene cation ($C_{16}H_{10}^{+}$) are shown in (e) and (f) as stick diagrams for comparison. The SPIRE spectrum in (b) matches well with both the matrix absorption (see Ref. 7) spectrum (e) and the gas-phase absorption (see Ref. 12) spectrum (f), except for the bands near 5.8–6.1 and 7.7–7.8 $\mu$m, marked with asterisks. The UIR spectrum from a planetary nebula, BD+30°3639 in this region is also shown in (a) for comparison.

Fig. 7(c) was obtained when the ions were deflected before entering the monochromator field of view under the same conditions.

IR emission in Fig. 7(b) is attributed to cationic species generated by electron impact of pyrene vapor for the following reasons. First, the ion optics and quadrupole electric field retard any *anions* moving toward the reflectron region, according to SIMION ion beam simulation. Therefore, anionic species cannot contribute to our spectra. Second, the ion current was measured at the last ring of the stack closest to the monochromator when the cations were injected into the reflectron region. Therefore, gas-phase cations definitely exist at the monochromator field of view during the signal scan. Third, the background spectrum in Fig. 7(c), which was obtained when the ion current was almost zero in the monochromator field of view, is essentially flat over the entire spectral range studied. If excited *neutral* species induced by electron impact had emitted IR radiation in the spectral range studied, the background spectrum would have shown some spectral features due to those species. Fourth, the IR spectrum of the pyrene cation shows very different features from that of neutral pyrene, and the major features observed in our emission spectrum in Fig. 7(b), except for extra bands in the 5.8–6.1 (1639–1724 $cm^{-1}$) and 7.7–7.8 $\mu$m (1282–1299 $cm^{-1}$) ranges, agree well with the calculated IR spectrum,[9] cryogenic matrix IR absorption spectra,[7,8] and gas-phase IR absorption spectrum[12] of the pyrene cation ($C_{16}H_{10}^{+}$), as shown in Fig. 7. The SPIRE spectrum in Fig. 7(b) can thus be attributed primarily to the pyrene monocation ($C_{16}H_{10}^{+}$).

Three bands at 5.81 $\mu$m (=1721 $cm^{-1}$), 5.90 (=1695 $cm^{-1}$), and 6.04 $\mu$m (=1656 $cm^{-1}$) in Fig. 7(b) can tentatively be assigned to a benzyne triple bond of the dehydrogenated pyrene cations. A strong band at 7.83 $\mu$m (=1277 $cm^{-1}$), with a shoulder at 7.74 $\mu$m (=1291 $cm^{-1}$) in Fig. 7(b) may be due to aromatic CC stretching vibrations of dehydrogenated pyrene cations that are redshifted from the strongest $C_{16}H_{10}^{+}$ band at 7.44 $\mu$m (1343 $cm^{-1}$). The gas-phase SPIRE spectrum of the neutral pyrene reported previously is shown in Fig. 7(d). Also the UIR spectrum from a planetary nebula, BD+30°3639 in this region is shown in Fig. 7(a) for comparison. A detailed data analysis was published elsewhere.[34]

## ACKNOWLEDGMENTS

This work was funded by the National Aeronautics and Space Administration Astrophysics (Grant No. NAG5-9384) and Exobiology (Grant No. NAG5-7457) programs. H.-S. K. thanks the Korea Research Foundation for financial support. The authors thank Dr. Stephan Schlemmer for a careful reading of this manuscript.

[1] M. D. Petroff, M. G. Stapelbroek, and W. A. Kleinhans, Appl. Phys. Lett. **51**, 406 (1987).
[2] A. Léger and J. L. Puget, Astron. Astrophys. **137**, L5 (1984); L. J. Allamandola, A. G. G. M. Tielens, and J. R. Barker, Astrophys. J. **290**, L25 (1985).
[3] D. J. Cook, S. Schlemmer, N. Balucani, D. R. Wagner, J. A. Harrison, B. Steiner, and R. J. Saykally, J. Phys. Chem. A **102**, 1465 (1998).
[4] D. J. Cook, S. Schlemmer, N. Balucani, D. R. Wagner, B. Steiner, and R. J. Saykally, Nature (London) **380**, 227 (1996).
[5] S. Schlemmer, D. J. Cook, J. A. Harrison, B. Wurfel, W. Chapman, and R. J. Saykally, Science **265**, 1686 (1994); D. R. Wagner, H.-S. Kim, and R. J. Saykally, Astrophys. J. **545**, 854 (2000).
[6] D. R. Wagner, Ph.D. thesis, University of California at Berkeley, 2001.
[7] D. M. Hudgins and L. J. Allamandola, J. Phys. Chem. **99**, 3033 (1995).
[8] M. Vala, J. Szczepanski, F. Pauzat, O. Parisel, D. Talbi, and Y. Ellinger, J. Phys. Chem. **98**, 9187 (1994).
[9] S. R. Langhoff, J. Phys. Chem. **100**, 2819 (1996).
[10] A. Léger and L. d'Hendecourt, Ann. Phys. (Paris) **14**, 181 (1989); L. J. Allamandola, A. G. G. M. Tielens, and J. R. Barker, Astrophys. J., Suppl. Ser. **71**, 733 (1989).
[11] J. Oomens, B. G. Sartakov, A. G. G. M. Tielens, G. Meijer, and G. von Helden, Astrophys. J. **560**, L99 (2001).
[12] J. Oomens, A. J. A. van Roij, G. Meijer, and G. von Helden, Astrophys. J. **542**, 404 (2000).
[13] H.-S. Kim, D. R. Wagner, and R. J. Saykally, Phys. Rev. Lett. **86**, 5691 (2001).
[14] M. E. Wacks, J. Chem. Phys. **41**, 1661 (1964).
[15] A. G. G. M. Tielens, Astrophys. Space Sci. **251**, 1 (1997).
[16] C. Joblin, L. d'Hendecourt, A. Léger, and D. Défourneau, Astron. Astrophys. **281**, 923 (1994).
[17] D. Rouan, A. Léger, A. Omont, and M. Giard, Astron. Astrophys. **253**, 498 (1992).
[18] C. E. Brion and A. Hamnett, Adv. Chem. Phys. **45**, 2 (1981).
[19] J. W. Keller, M. A. Coplan, and R. Goruganthu, Astrophys. J. **391**, 872 (1992).
[20] S. F. Wong and G. J. Schulz, Phys. Rev. Lett. **35**, 1429 (1975).
[21] M. A. Khakoo, J. M. Ratliff, and S. Trajmar, J. Chem. Phys. **93**, 8616 (1990).
[22] J. P. Maier and O. Marthaler, Chem. Phys. **32**, 419 (1978).
[23] K. Furuya, E. Koto, and T. Ogawa, Chem. Phys. Lett. **253**, 87 (1996).
[24] C. Engelhardt, J. C. Keske, F. S. Rees, Y. B. Self-Medlin, H. S. Yoo, and B. H. Pate, J. Phys. Chem. A **105**, 6800 (2001).
[25] C. M. White, J. Chem. Eng. Data **31**, 198 (1986).
[26] J. Kirschner, Rev. Sci. Instrum. **57**, 2640 (1986).

[27] V. W. Lippert and W. Pohlit, Optik (Stuttgart) **9**, 456 (1952).
[28] D. A. Dahl, SIMION three-dimensional version 6.0 (1995).
[29] H. D. Zeman, Rev. Sci. Instrum. **48**, 1079 (1977).
[30] A. Ding, K. Richter, and M. Menzinger, Chem. Phys. Lett. **77**, 523 (1981).
[31] J. V. Coe, J. C. Owrutsky, E. R. Keim, N. V. Agman, D. C. Hovde, and R. J. Saykally, J. Chem. Phys. **90**, 3893 (1989); J. C. Owrutsky, E. R. Keim, J. V. Coe, and R. J. Saykally, J. Phys. Chem. **93**, 5960 (1989).
[32] J. W. Farley, Rev. Sci. Instrum. **56**, 1834 (1985).
[33] S. Leach, Z. Phys. Chem. (Munich) **195**, 15 (1996).
[34] H.-S. Kim and R. J. Saykally, Astrophys. J., Suppl. Ser. **143**, 455 (2002).